Hybrid microwave sintering of alumina and 3 mol% Y2O3-stabilized zirconia in a multimode cavity – Influence of the sintering cell

Nouhaila Khalile, Clémence Petit, Christophe Meunier, François Valdivieso

Hybrid microwave sintering of alumina and 3 mol% Y_2O_3-stabilized zirconia in a multimode cavity – Influence of the sintering cell

Nouhaila Khalile, Clémence Petit*, Christophe Meunier, François Valdivieso

Mines Saint-Etienne, Univ Lyon, CNRS, UMR 5307 LGF, F-42023 Saint-Etienne France

* Corresponding author: Clémence Petit (email: clemence.petit@emse.fr)

Mines Saint-Etienne, Univ Lyon, CNRS, UMR 5307 LGF, F-42023 Saint-Etienne France

Abstract

In microwave (MW) sintering, samples directly heat by absorption of the electromagnetic field, leading to a fast volumetric heating. Thus, the materials are heated thanks to their own dielectric properties. In multimode cavities, samples are always heated with a sintering cell in order to get an insulation of the samples and a heating homogeneity. However, to date, very limited research has been carried out to study the effects of materials used in the sintering cell. In this paper the microstructure and densification of Al_2O_3 and 3Y-TZP were investigated and compared between three different sintering cells. The used sintering cell contains three main elements: thermal insulators, a SiC susceptor and a protective mullite tube. Higher final densities (98.3±0.6% and 98.6 ±0.6% of T.D. for Al_2O_3 and 3Y-TZP respectively), lower densification temperatures and better microstructure homogeneity were obtained by using the sintering cell containing both mullite tube and SiC susceptor. But, sintering using the sintering cell without the SiC susceptor was also possible, especially for the lowest lossy material,*i.e.*, Al_2O_3. This can be explained by a possible susceptor effect of the mullite tube. However, the microstructural observations showed a difference of homogeneity in the microstructure for Al_2O_3 and 3Y-TZP with some sintering cells. It can be linked to the difference of dielectric properties of the two materials. The influence of the sintering cell is less critical for 3Y-TZP, which couples better with MW than Al_2O_3. It was also observed that densification curves were

switched to higher temperatures during sintering with the presence of SiC susceptor and without mullite tube. These results were justified by an error in the temperature measurement of the IR-pyrometer.

Keywords: Alumina, Yttria-stabilized zirconia, Microwave sintering, Susceptor, Sintering cell

1. Introduction

Ceramics are widely used in several applications. These materials demonstrate advantageous properties such as high temperature stability, corrosion resistance, wear resistance and attractive mechanical properties. Alumina (Al_2O_3), zirconia (ZrO_2) and bioactive ceramics (*i.e.*, calcium phosphates) are, today, the most known and used ceramics especially in biomedical applications [1–3]. Ceramic processing involves three main steps: synthesis of powders, shaping and sintering. In general, conventional (CV) sintering consumes a high amount of energy and time due to the long duration and high temperatures required. Meanwhile novel processes as Spark Plasma Sintering (SPS) [4,5], induction sintering [6,7], flash sintering [8,9] and microwave (MW) sintering [10] were developed in order to be faster and more efficient. MW sintering has been studied in recent decades and it is considered as an interesting alternative method of sintering for fabrication of ceramic materials [10]. In MW sintering, the material interacts directly with the electromagnetic field, causing a volume heating of the samples [11]. Consequently, it leads to higher heating rates and to a uniform temperature distribution within the solid. Compared to CV sintering, MW sintering can reduce processing times and lead to energy savings [10,11]. Under MW field, a material heats by its own dielectric properties. Two principal dielectric properties are responsible of coupling capability of materials: the complex permittivity (ε^*) and the loss tangent (tan α) [12]. ε^* can be defined by the following formula: $\varepsilon^* = \varepsilon' - j\varepsilon''$ where ε' is the dielectric constant and ε'' is the dielectric loss factor. The loss tangent is defined as $\tan(\alpha) = \varepsilon''/\varepsilon'$. The higher dielectric loss factor, the more material couples with the electromagnetic field (EM) and heats up quickly.

For an effective MW sintering, samples must always be placed in an insulation box. This insulation system contains the susceptor and thermal insulators. The latter are used to minimize heat losses from the sample and the susceptor by conduction and radiation. Alumina or aluminosilicate based materials are usually used as thermal insulators because they follow the

main requirements for MW applications: transparency to microwave, stability at high temperature and low thermal conduction [13]. To ensure better insulation, some studies have used multilayer thermal barriers of materials that remain transparent in microwaves above 1000°C [14]. Even if these thermal insulators used in the sintering cell are chosen for their transparency, some studies showed that they can absorb a part of the MW. For example, Garnault *et al.* [15] tested different sintering cells for MW sintering of Al_2O_3 and 3Y-TZP in a single-mode cavity. They demonstrated that the sintering cell could act as a susceptor in some conditions. The influence of the sintering cell can become more important when the sample is sintered in a multimode cavity. In this type of cavities, the weight of thermal insulators is generally higher than the weight of the sample to sinter. Therefore, the influence of the sintering cell is possibly more important in a multimode cavity, compared to a single-mode one.

Many authors worked about microwave sintering of oxide ceramics, especially alumina and 3 mol% yttria tetragonal zirconia polycrystal (3Y-TZP) [16–18]. Literature shows that these materials are often sintered with the help of a susceptor. The susceptor is a material which strongly couples with MW and can transmit heat to the sample, mainly via radiation [13]. In the case where a susceptor is used, MW heating is called hybrid or indirect heating. Silicon carbide (SiC) is often used as a susceptor to sinter materials with low dielectric loss as Al_2O_3 [19] or materials with brutal changes of dielectric properties as 3Y-TZP. This later couples better with MW than Al_2O_3 but its loss tangent increases sharply with temperature [20,21]. Without susceptor, this behavior can create difficulties to control its heating rate under MW, and thus to control the sintering cycle [15,22].

The susceptor can take different shapes as rod-like (picket fence arrangement), tubular, rings or powdered form. The advantage of the picket fence arrangement is that the positioning of these rods does not make a screen to MW due to the gap between the used bars. This gap is generally filled with the insulation material in order to prevent heat loss. Janney *et al.* [23] sintered

zirconia samples with a direct and indirect configuration in a 2,45 GHz MW cavity. In this study, they used a "picket fence" arrangement in order to provide a hybrid MW sintering of zirconia samples. In this arrangement, the samples were surrounded by SiC rods and zirconia bulk fiber insulation [23]. Compared to the direct sintering, using the picket fence allowed to achieve higher final densities and to prevent crack during sintering. Powdered susceptor was also very used for alumina and zirconia MW sintering [14]. In this case, the samples are embedded within the susceptor powder. The quantity of susceptor powder should be determined in order to ensure that the sample was adequately exposed to the electric field. Ramesh *et al.* used this type of susceptor for alumina and zirconia hybrid MW sintering [14]. High densities of 99% and above 95 % were achieved for yttria stabilized zirconia and alumina, respectively [24]. Then, susceptors with a tubular configuration were used but presented some problems [24]. The tube surrounding the samples can lead to a screen effect for MW. Zhao *et al.* [25] used a tubular SiC susceptor during a single mode cavity sintering of alumina and zirconia. They demonstrated that MW can partially penetrate the thin susceptor and give a hybrid sintering of the ceramics. Nowadays, the most used susceptors are rings [16] and plates [26].
The nature of susceptor can also have an influence on the efficiency of the hybrid MW sintering. Heuguet *et al.* studied the influence of the materials used as susceptor to sinter alumina [27]. They demonstrated that a zirconia susceptor favors a direct MW/alumina interaction whereas a SiC susceptor leads to a mainly indirect heating.

As reported above, various studies of MW sintering of ceramics have been performed with different types of sintering cells (*i.e.,* materials, geometries). But, the influence of these sintering cells is more rarely addressed. It has to be noted that the use of MW sintering at industrial scale is possible in 2,45 GHz multimode cavities because their dimensions enable to sinter large pieces (contrary to single-mode cavities). Therefore, understanding the role of each

material placed in the cavity is important in order to optimize the design of future cavities and sintering cells.

The aim of this work is to study the effect of a sintering cell during MW sintering of alumina and zirconia in a multimode cavity. Alpha alumina (α-Al_2O_3) and 3Y-TZP were chosen due to their different dielectric behavior as mentioned previously. This work was performed in a MW instrumented cavity designed during previous studies [15,27]. This MW device allows for heating ceramic materials with a precise control of heating cycles and it is equipped with pyrometers and optical dilatometry to monitor sintering [28]. The sintering cell used in this work contains different elements and was also designed during previous studies [20,21]. Alumina and 3Y-TZP pellets were sintered in this cavity, using different configurations of the sintering cell. The sintered materials were characterized in terms of final densities and grain sizes.

2. Experimental procedures

2.1. Samples preparation

High purity (99.999%) commercial α-Al_2O_3 powder with an average particle size of 125 nm and a specific surface area of 15 m^2/g (*BMA-15, Baikowski International, France*) and 3Y-TZP powder (99.99% of purity, *TOSOH Corporation, Japan*) with an average particle size of 40 nm and a specific surface area of 16 m^2/g, were used as starting materials. The compositions of α-Al_2O_3 and 3Y-TZP powders are given in **Erreur ! Source du renvoi introuvable.** and **Erreur ! Source du renvoi introuvable.**, respectively. The powders were prepared by colloidal process. The suspensions were prepared by adding the powders to an aqueous solution of 2.7 wt% of dispersant (*DARVAN CN, Vanderbilt minerals, LLC*). The pH of the solution was adjusted to 10 by addition of NaOH. After adding of 2 wt% of polyvinyl alcohol (PVA) binder (*Rhodoviol 4/125; Prolabo, France*) and 1 wt% polyethylene glycol (PEG) plasticizer (*Mw 1500; Prolabo,*

France), the suspensions were ball-milled using 2 mm Al_2O_3 balls for 18 hours. Finally, the suspensions were spray-dried with a spray-dryer (*Mini Spray-Dryer Buchi 190*)

The spray-dried powders were shaped into disks by uniaxial pressing (12 mm diameter with 4 mm thickness) at 50 MPa and then isostatically pressed at 300 MPa. The organic additives were removed with a heating treatment at 1°C/min up to 600°C with a dwell of 1 hour in air. The green bodies had a density from 50% to 53% of T.D (theoretical densities, which are 3.987 g/cm^3 and 6.07 g/cm^3 for Al_2O_3 and 3Y-TZP, respectively).

2.2. The multimode MW cavity

MW sintering experiments were performed in an instrumented MW heating system designed and described by Zymełka *et al.* [39]. The main elements of the device are presented in this section: the cavity itself, the pyrometer, the optical dilatometry and the Labview software.

The MW furnace was a multimode cuboid cavity (dimensions of 430 mm × 430 mm × 490 mm). MW were produced by a magnetron powered by a 3kW generator (*GMP30K, SAIREM, France*) working at a fixed frequency of 2.45 GHz. This cavity was equipped with a IR pyrometer to follow the thermal cycle and a CCD camera to follow the shrinkage.

A bichromatic pyrometer (*Lumasense Technology, Germany*) sensitive to the wavelength between 2 and 2.5 µm, working in the 250-1800 °C temperature range was used. To obtain an accurate value of temperature, it is necessary to know the ratio of apparent emissivity *k* in the experimental conditions. Therefore, a calibration method based on the melting point of a metallic calibration material was used as described by Zymełka *et al.* [28,29]. In this study, palladium (melting temperature of 1550 °C) was used as the calibrating material. A small amount of this material was inserted in a small hole engraved in the sample's surface. When the metal started to melt, the ratio *k* of the pyrometers was calculated to match the pellet temperature with the one of the palladium melting temperature. The calculated average values of the ratio *k* were 1.01 and 0.9547 for Al_2O_3 and 3Y-TZP, respectively.

Optical dilatometry was used to record the pellet's shrinkage during sintering. The procedure used in this work was previously described by Zymelka *et al.* [28], Zuo *et al.* [16] and Meunier *et al.* [30]. A high-resolution CCD camera (*SLC2050MTLGEC; 14-bit, 1600 9 1200, SVS-VISTEK, Seefeld, Germany*), recorded pictures of the flat circular surface of the pellet during the thermal cycle. Then, the recorded images were processed by a dedicated homemade Labview® software (*National Instruments, USA*) which detected the pellets' edges to measure the diameter. The program finally output the evolution of the pellet's diameter during sintering. Then, these data were used to plot the evolution of the instantaneous density versus temperature. For this purpose, the instantaneous density during sintering was calculated thanks to Eq. 1, taking into account the anisotropy shrinkage ratio α (Eq. 2).

$$\rho(t) = \frac{\left(1+\frac{h_f-h_0}{h_0}\right)*\left(1+\frac{D_f-D_0}{D_0}\right)^2}{\left(1+\frac{1}{\alpha}*\frac{D(t)-D_0}{D_0}\right)*\left(1+\frac{D(t)-D_0}{D}\right)^2} * \rho_f \quad \text{(Eq. 1)}$$

$$\alpha = \frac{D_f-D_0}{D_0} * \frac{h_0}{h_f-h_0} \quad \text{(Eq. 2)}$$

Where $\rho(t)$ is the instantaneous density of the sample, ρ_f the final density, h_f the final height, h_0 the initial height, D_f the final diameter, D_0 the initial diameter and $D(t)$ the instantaneous diameter.

The thermal cycle was controlled by a specific homemade LabVIEW software. It used a PID controller based on the temperature measured by the pyrometer. The incident power delivered by the generator was continuously adjusted during the sintering cycle to match the measured temperature with the set temperature. It also recorded the data (microwave power, temperature, images) useful to control the thermal treatment and to plot the dilatometric curves.

2.3. The sintering cell

The green samples were positioned in a sintering cell (Figure 1) in order to optimize their insulation and guarantee their homogeneous heating. The sintering cell used in this study was mainly made of different plates of aluminosilicate fibers (*KVS 184–400, RATH®, Germany*) as thermal insulator. This material was used because it meets the requirements of MW applications: transparency to MW, stability at high temperature (to 1800 °C) and low thermal conductivity (0.33 $W.m^{-1}.K^{-1}$ at 1400 °C). Inside the cell, the sample was placed on two alumina sample holders to record images of its flat surface. A SiC ring was used as susceptor to initiate samples' heating. A low lossy mullite tube (C610, AMTS, France) surrounded the sample. This tube was used to minimize the susceptor radiation to the sample at high temperature.

2.4. Sintering experiments and samples characterization

The MW thermal cycles were performed in the multimode cavity described in the section 2.2. In order to study the influence of the elements of the sintering cell, the samples were sintered with three different sintering cells presented in Table 3. The three different sintering cells contained the thermal insulators and differed by the presence or absence of the SiC ring and the mullite tube. Table *5* describes the three sintering cells, noted S, M and SM.

The following thermal cycle was applied for all the MW sintering experiments: heating to 1550°C at a heating rate of 25°C/min and a dwell time of 10 min at the peak temperature. A unique thermal cycle was used for Al_2O_3 and 3Y-TZP to facilitate the comparison between them. The sintering temperature was chosen according to dilatometric experiments carried out in a conventional dilatometer with the pellets, not shown here. Densities were measured by Archimedes' method with absolute ethanol as the liquid medium. Theoretical densities of 3.987 $g.cm^{-3}$ and 6.07 $g.cm^{-3}$ were used to calculate the relative densities for Al_2O_3 and 3Y-TZP,

respectively. The microstructures were observed using Scanning Electronic Microscopy (SEM, *Zeiss SUPRA55VP, Carl Zeiss Microscopy GmbH, Oberkochen, Germany*). Before observation, the samples were cut, polished until mirror surface finishing and thermally etched at 1480 °C during 10 min. The average grain sizes of Al_2O_3 and 3Y-TZP samples were measured by image analysis using the ImageJ software by the linear intercept method on at least 400 grains. This was carried out at different locations on the cut surface (near the surface and in the center).

3. Results

3.1. Power evolution during sintering

Figure 2 and Figure 3 present the evolution of temperature, incident (*Pi*) and absorbed (*Pabs*) MW powers during the sintering cycles of Al_2O_3 and 3Y-TZP, respectively for the various sintering cells.

Figure *9*(a) compares the power evolution during sintering of Al_2O_3 between the SM and M sintering cells. It can be noticed that heating started earlier with the presence of the susceptor.

Without the susceptor (sintering cell M), the samples needed higher *Pi* and longer time (1200 W and 19 min) to start heating in comparison with the sintering cell SM (600 W and 5 min) (Figure 3(a)). The *Pi* value is lower with the sintering cell SM compared to the sintering cell M until 1360 °C. Then at higher temperatures, *Pi* for the sintering cell SM increased and became higher compared to *Pi* with the sintering cell M. This latter value is almost stable for the three sintering cycles after the beginning of the heating. The *Pabs* values follow the same tendency as the incident power. Before the beginning of the heating, the absorbed power is the highest for the sintering cell M. From a temperature of around 1360 °C, the *Pabs* values for the sintering cell SM increased and became higher than for the sintering cell M.

The comparison of the sintering cells SM and S (

Figure *9* (b)) shows that without the mullite tube, heating starts immediately after the beginning of the heating. Then, the *Pi* and *Pabs* values are lower during the whole thermal cycle without the mullite tube (

Figure *9* (b)).

For the 3Y-TZP sample (see Figure 3), the effect of the susceptor is the same as observed for the Al_2O_3 sample. Both samples needed lower values of *Pi* and shorter time to start heating with the sintering cell SM in comparison with the sintering cell M (Figure 3(a)). Heating starts after only 3 min with only 200 W with the use of the SiC susceptor, while for the sintering cell M, the beginning of the heating takes more time (14 min) and needs a higher power (1200 W). In the figure 3(a), it is observed that during almost the entire cycle of sintering with the sintering cell SM, the *Pi* values are lower than for the sintering cell S. Figure 3(a) also shows that the absorbed power is higher in the case of the sintering cell M until the temperature of 566 °C when it becomes almost equal to the values measured with the sintering cell SM.

With the sintering cell S (Figure 3(b)), the heating starts immediately with a lower incident power in comparison with the sintering cell SM. The incident power is lower when the sintering cell S is used in comparison with the sintering cell SM until 1250 °C. At this temperature, it increased until the end of the thermal cycle. The situation is similar for the absorbed power: the

values are the lowest ones in the case of the sintering cell S at the beginning of the heating and becomes the highest one when the peak temperature is reached.

3.2. Densification behavior

Figure 4 shows the densification curves for each material with the three sintering cells. For the Al_2O_3 samples, the densification started at the temperatures of about 1045 °C, 1150 °C and 1330 °C for the cells SM, M and S, respectively (Figure 4(a)). The temperature of the onset densification of the 3Y-TZP samples are about 1000 °C for the sintering cells SM and M and about 1290 °C for the sintering cell S (Figure 4(b)). This difference of temperature between the various sintering cells is observed for the initial and intermediate stages of sintering. But, during the final stage of sintering (relative density > 90 %), this difference between the densification curves decreases. This is confirmed by the final relative densities of the sintered samples (

Table *6*). All the samples have a high relative density (> 97.5 %). No significant difference can be found between the different sintering cells for a given material.

Table 7 presents the temperatures at which a relative density of 75 % is reached (corresponding to the intermediate stage of sintering) for the different sintering cells and for both materials. The difference of these temperatures for two sintering cells is also presented. The difference of temperature between the sintering cells SM and M ($\Delta T_{M\text{-}SM}$ in Table 3) shows that the presence of the SiC susceptor enables to densify at a lower temperature in the intermediate stage of sintering. The difference of temperature between the sintering cells S and SM also shows that the densification took place at a higher temperature without the mullite tube. The sintering cells S and M both led to a higher temperature needed to reach a relative density of 75 %, in comparison with the sintering cell SM. But, the effect of the mullite tube on the temperature is more important than that of the SiC ring. Moreover, the effect of the sintering cell is different for the two materials. For example, the $\Delta T_{M\text{-}SM}$ value is higher for the Al_2O_3 pellet than that of the 3Y-TZP pellet.

3.3. Microstructure of sintered samples

The SEM observations were carried out in order to study Al_2O_3 and 3Y-TZP microstructures and average grain size evolution.

Figure *11* and **Erreur ! Source du renvoi introuvable.** show the SEM images of the Al_2O_3 and 3Y-TZP pellets respectively, sintered with the three sintering cells. For each sample, representative images taken near the surface and in the center of the polished surface are presented.

The sintered Al_2O_3 pellets present a bimodal grain size distribution with a grain size in the range 1-2 µm. Some abnormally grown grains are visible (see

Figure *11*a and 5b). The presence of some pores in the sintered Al_2O_3 sample with the sintering cell M (

Figure *11* (b) and 5 (e)) can be linked with its slightly lower final relative density (see Table 5).

In the opposite, the 3Y-TZP pellets present a very fine microstructure with grain sizes in the

submicrometer range (from 0.35 to 0.46 µm) with almost similar microstructures with the three sintering cells (**Erreur ! Source du renvoi introuvable.**).

Figure 7 presents the Al_2O_3 and 3Y-TZP average grain sizes and standard deviations for the different sintering cells. A higher difference of average grain sizes between the surface and the center of the samples is visible for the Al_2O_3 samples, compared with the 3Y-TZP ones. This difference is more pronounced when the Al_2O_3 pellet was sintered with the sintering cells M and S. Conversely, it is low when the specimen was sintered with the sintering cell SM. A slightly higher average grain size was reached in the center than at the surface for the two sintering cells with the SiC ring. Instead, the average grain size is slightly higher at the surface with the sintering cell M. A standard deviation of the grain size of around 1 µm is observed for the three sintering cells. For the 3Y-TZP samples, a more homogeneous microstructure is obtained whatever the sintering cell used. The standard deviation of the grain size distribution is only around 0.2 – 0.4 µm.

4. Discussion

4.1. Effect of the SiC susceptor

The results obtained with the sintering cell S shows that the densification curves are shifted to higher temperatures. This result can be at first eyesight surprising because a lot of authors used sintering cells containing only thermal insulators and SiC and demonstrated lower densification temperature. These results can be explained by the radiation of the SiC received by the sample. This can lead to errors in the temperature measurement given by the pyrometers, in relation with the values of emissivity ratio in the different sintering cells. In order to make sure about this hypothesis, a new calibration of the IR-pyrometer with the 3Y-TZP sample has been done using the sintering cells S and M (

Table *8*). Comparing the sintering cells SM and M, the ratio *k* is almost similar. It means that the environment of the sample was quite similar in the presence of the mullite tube. Conversely, the recalculated ratio *k* was higher (*k* = 1.111) for the sintering cell S in comparison with the sintering cell SM. In this case, when the calibration material started melting, the measured temperature was 1672 °C with *k* = 0,955 while the value should have been at 1550 °C (melting temperature of palladium). Thus, the densification curves shown in Figure 4 for the sintering cell S have probably an offset of temperature related to an error in temperature measurement

by the pyrometer. This highlights the possible important role of the mullite tube in the sintering cell, as a protective element from the SiC radiations.

4.2. Effect of the mullite tube

Direct MW heating of ceramic materials with low dielectric properties such as Al_2O_3 in a multimode MW cavity is often viewed as impossible. However, in this study, the Al_2O_3 sample was sintered until full densification in the multimode cavity with the sintering cell M (*i.e.*, without the SiC susceptor). This could be explained by a probable susceptor effect of the mullite tube. It can be linked to a probable variation of its dielectric properties with temperature. Samuels et *al.* show that the dielectric loss tangent of ceramics such as Al_2O_3 increases with temperature [31]. It can be hypothesized here that such a variation also occurs to mullite. Consequently, this transparent material at ambient temperature can become a MW absorber at higher temperature. The 3Y-TZP pellets was also successfully sintered without the SiC susceptor. The heating cycle of 3Y-TZP was correctly controlled and no hot spot was observed with the sintering cell M. However, these problems are often observed during direct MW sintering of 3Y-TZP [14] and often justify the use of an external susceptor [21]. Therefore, sintering of the 3Y-TZP pellet with the sintering cell M cannot be considered as a direct MW sintering. This confirms that the mullite tube plays a role of susceptor in the sintering cell. But, it acts as a less efficient susceptor than the the SiC ring. This is supported by the higher temperature needed to reach a given relative density (

Table *7*) using the sintering cell M in comparison with the sintering cell SM.

Moreover, the comparison between the different sintering cells and the two materials highlights the difference of coupling capability between alumina and zirconia. These differences are visible even in a multimode cavity. Figure 4 shows that the densification curves of the 3Y-TZP pellets with the sintering cells SM and M were almost similar. This can be linked to the high dielectric loss tangent of yttria-stabilized zirconia. Thus, it is not influenced by the efficiency of the susceptor. This is not the case for the Al_2O_3 specimen for which the densification curve with the sintering cell M is shifted to the higher temperatures. It highlights the importance of the careful choice of the sintering cells and especially of the susceptors for the low coupling materials.

4.3. Effect of the sintering cell on the microstructure

The Al_2O_3 grain size was quite affected by the change of the sintering cell. On the contrary, the difference of grain sizes between the center and the surface is smaller for the 3Y-TZP pellets. A more homogeneous microstructure between the center and the surface of Al_2O_3 is obtained with the sintering cell SM, in comparison with the two other ones (as shown in

Figure *11*). This homogeneity and lower densification temperatures can be related to the combined effect of a double susceptor effect of SiC and the mullite tube. The positioning of the sample inside the mullite tube probably helps to obtain homogeneous heating which can explain the more homogeneous microstructure obtained with the sintering cell SM. It confirms the important effect played by the sintering cell, as already pointed out the section 4.2.

With the sintering cell M, the average grain size of Al_2O_3 at the surface is higher than the one in the center. This result confirms the susceptor effect of the mullite tube. When the mullite tube acts as a susceptor, the surface remains at higher temperature, which can explain the higher grain size in this area of the sample. However, in the case of the sintering cell S, the average grain size in the center of the sintered sample is higher than the one in the surface. It means that the bulk of the sample was hotter than the surface. But, the electromagnetic field usually heats preferentially the SiC ring, which then heats the samples by radiation. Thus, it should have led

to a higher temperature at the surface and so, to a higher average grain size at the surface. The hypothesis of a higher MW/alumina interactions leading to a bulk heating is unlikely because of the dielectric properties of alumina and of the presence of the SiC ring. In this case, the simulation of the propagation of the electromagnetic field with these sintering cells could help to understand this reverse effect with the sintering cell S. For these materials, the sintering cell SM seems the best choice to combine the SiC susceptor and the protective role of mullite.

Probably due to its high dielectric loss tangent, the microstructure and densification behavior of 3Y-TZP is less affected by the change of the sintering cell. In particular, MW sintering of 3Y-TZP with or without the SiC ring (sintering cells SM and M, see Figure 4 and Figure 7) led to similar results in terms of densification curves, final density and microstructure.

5. Conclusion

The aim of this paper was to investigate the effect of materials of the sintering cell on the microstructure and the densification of the samples. For this purpose, Al_2O_3 and 3Y-TZP pellets were sintered in a MW multimode instrumented cavity with three different sintering cells. The sintering cell contains three elements: thermal insulators, a SiC ring used as susceptor and a protective mullite tube.

Our results highlight the importance of a careful choice of the material constituting the sintering cell, in relation with the material to sinter. This is particularly important for the use of MW sintering at an industrial scale, for which multimode cavity is the only possible cavity to sinter large pieces. The sintering experiments with Al_2O_3 and 3Y-TZP confirm that the presence of SiC and mullite tube contributes to a homogeneous heating of the pellets, leading to a homogeneous microstructure. The sintering cell M allows for a heating without thermal runaway for 3Y-TZP and a homogeneous microstructure of both Al_2O_3 and 3Y-TZP pellets. It shows that the absence of the SiC ring did not lead to a direct MW sintering. The mullite tube

probably plays the role of susceptor and helps to obtain a homogeneous heating, even if it couples less with MW than SiC. The densification curves and the grain size values show that Al_2O_3 was more affected by the efficiency of the external susceptor.

Deeper investigations could be carried out to better understand the role of the mullite tube. In particular, the thermal cycles performed with the sintering cell with the SiC ring and without the mullite tube were not helpful because of a probable error in the temperature measurement. Simulations of the propagation of the electromagnetic field with different sintering cells could also be interesting to complete the experimental work. Furthermore, other materials could be tested to play the role of thermal insulator, protective tube and susceptor.

6. References

[1] J. Chevalier, L. Gremillard, Ceramics for medical applications: A picture for the next 20 years, J. Eur. Ceram. Soc. 29 (2009) 1245-1255. https://doi.org/10.1016/j.jeurceramsoc.2008.08.025.

[2] B.S. Bal, J. Garino, M. Ries, M.N. Rahaman, Ceramic materials in total joint arthroplasty, Semin. Arthroplasty. 17 (2006) 94-101. https://doi.org/10.1053/j.sart.2006.09.002.

[3] S.J. Kalita, A. Bhardwaj, H.A. Bhatt, Nanocrystalline calcium phosphate ceramics in biomedical engineering, Mater. Sci. Eng. C. 27 (2007) 441–449. https://doi.org/10.1016/j.msec.2006.05.018.

[4] Z.-Y. Hu, Z.-H. Zhang, X.-W. Cheng, Fu-ChiWang, Y.-F. Zhang, S.-L. Li, A review of multi-physical fields induced phenomena and effects in spark plasma sintering: Fundamentals and applications, Mater. Design 191 (2020) 108662. https://doi.org/10.1016/j.matdes.2020.108662

[5] E. Olevsky, D. Dudina, Sintering by low-voltage electric pulses (including Spark Plasma Sintering (SPS)). In: E. Olevsky, D. Dudina, *Field-Assisted Sintering: Science and Applications.* Springer International Publishing, pp. 89-191, 2018.

[6] B. Guenther, Electromagnetic Theory, In: B. Guenter, *Modern Optic*. Oxford University Press, pp. 15-51, 2015.

[7] E. Olevsky, D. Dudina, Induction Heating Sintering. In: E. Olevsky, D. Dudina, *Field-Assisted Sintering: Science and Applications*. Springer International Publishing, pp. 275-291, 2018.

[8] E. Olevsky, D. Dudina, Flash Sintering. In: *Field-Assisted. Sintering: Science and Applications*. Springer International Publishing, pp. 193-232, 2018.

[9] M. Biesuz, V.M. Sglavo, Flash sintering of ceramics, J. Eur. Ceram. Soc. 39 (2019) 115-143. https://doi.org/10.1016/j.jeurceramsoc.2018.08.048.

[10] D. Agrawal, J. Cheng, H. Peng, L. Hurt, K. Cherian, Microwave energy applied to processing of high-temperature materials, Am. Ceram. Soc. Bull. 87 (2008) 39-43.

[11] M. Oghbaei, O. Mirzaee, Microwave versus conventional sintering: A review of fundamentals, advantages and applications, J. Alloys Compd. 494 (2010) 175-189. https://doi.org/10.1016/j.jallcom.2010.01.068.

[12] R.R. Mishra, A.K. Sharma, Microwave–material interaction phenomena: Heating mechanisms, challenges and opportunities in material processing, Compos. Part Appl. Sci. Manuf. 81 (2016) 78-97. https://doi.org/10.1016/j.compositesa.2015.10.035.

[13] M. Bhattacharya, T. Basak, A review on the susceptor assisted microwave processing of materials, Energy. 97 (2016) 306-338. https://doi.org/10.1016/j.energy.2015.11.034.

[14] S. Ramesh, N. Zulkifli, C.Y. Tan, Y.H. Wong, F. Tarlochan, S. Ramesh, W.D. Teng, I. Sopyan, L.T. Bang, A.A.D. Sarhan, Comparison between microwave and conventional sintering on the properties and microstructural evolution of tetragonal zirconia, Ceram. Int. 44 (2018) 8922-8927. https://doi.org/10.1016/j.ceramint.2018.02.086.

[15] T. Garnault, D. Bouvard, J.-M. Chaix, S. Marinel, C. Harnois, Is direct microwave heating well suited for sintering ceramics?, Ceram. Int. 47 (2021) 16716-16729. https://doi.org/10.1016/j.ceramint.2021.02.242.

[16] F. Zuo, C. Carry, S. Saunier, S. Marinel, D. Goeuriot, Comparison of the microwave and conventional sintering of alumina: Effect of MgO doping and particle size, J. Am. Ceram. Soc. 96 (2013) 1732-1737. https://doi.org/10.1111/jace.12320

[17] S. Charmond, C.P. Carry, D. Bouvard, Densification and microstructure evolution of Y-Tetragonal Zirconia Polycrystal powder during direct and hybrid microwave sintering in a single-mode cavity, J. Eur. Ceram. Soc. 30 (2010) 1211-1221. https://doi.org/10.1016/j.jeurceramsoc.2009.11.014.

[18] Z. Xie, J. Yang, Y. Huang, Densification and grain growth of alumina by microwave processing, Mater. Lett. 37 (1998) 215-220. https://doi.org/10.1016/S0167-577X(98)00094-9.

[19] H. Curto, A. Thuault, F. Jean, M. Violier, V. Dupont, J.-C. Hornez, A. Leriche, Coupling additive manufacturing and microwave sintering: A fast processing route of alumina ceramics, J. Eur. Ceram. Soc. 40 (2020) 2548-2554. https://doi.org/10.1016/j.jeurceramsoc.2019.11.009.

[20] M. Arai, J.G.P. Binner, T.E. Cross, Comparison of techniques for measuring high-temperature microwave complex permittivity: measurements on an alumina/zircona System, J. Microw. Power Electromagn. Energy. 31 (1996) 12-18. https://doi.org/10.1080/08327823.1996.11688287.

[21] J. Batt, W.H. Sutton, J.G.P. Binner, T.E. Cross, A parallel measurement programme in high temperature dielectric property measurement: An update, (1995). https://www.osti.gov/biblio/269926 (accessed July 22, 2021).

[22] C. Manière, T. Zahrah, E.A. Olevsky, Fully coupled electromagnetic-thermal-mechanical comparative simulation of direct vs hybrid microwave sintering of 3Y-ZrO_2, J. Am. Ceram. Soc. 100 (2017) 2439-2450. https://doi.org/10.1111/jace.14762.

[23] M.A. Janney, C.L. Calhoun, H.D. Kimrey, Microwave sintering of solid oxide fuel cell materials: I, Zirconia-8 mol% yttria, J. Am. Ceram. Soc. 75 (1992) 341-346. https://doi.org/10.1111/j.1151-2916.1992.tb08184.x.

[24] J. Lasri, L. Schachter, Energy flow during microwave sintering of zirconia in the presence of a SiC susceptor. In: *MELECON '98. 9th Mediterranean Electrotechnical Conference. Proceedings***.** IEEE, pp. 236-240, 1998.

[25] C. Zhao, J. Vleugels, C. Groffils, P.J. Luypaert, O. Van Der Biest, Hybrid sintering with a tubular susceptor in a cylindrical single-mode microwave furnace, Acta Mater. 48 (2000) 3795-3801. https://doi.org/10.1016/S1359-6454(00)00160-9.

[26] S. Marinel, C. Manière, A. Bilot, C. Bilot, C. Harnois, G. Riquet, F. Valdivieso, C. Meunier, C. Coureau, F. Barthélemy, Microwave sintering of alumina at 915 MHz: modeling, process control, and microstructure distribution, Materials. 12 (2019) 2544. https://doi.org/10.3390/ma12162544.

[27] R. Heuguet, S. Marinel, A. Thuault, A. Badev, Effects of the susceptor dielectric properties on the microwave sintering of alumina, J. Am. Ceram. Soc. 96 (2013) 3728-3736. https://doi.org/10.1111/jace.12623.

[28] D. Żymełka, S. Saunier, J. Molimard, D. Goeuriot, Contactless monitoring of shrinkage and temperature distribution during hybrid microwave sintering, Adv. Eng. Mater. 13 (2011) 901-905. https://doi.org/10.1002/adem.201000354.

[29] D. Żymełka, S. Saunier, D. Goeuriot, J. Molimard, Densification and thermal gradient evolution of alumina during microwave sintering at 2.45GHz, Ceram. Int. 39 (2013) 3269-3277. https://doi.org/10.1016/j.ceramint.2012.10.015.

[30] C. Meunier, F. Zuo, N. Peillon, S. Saunier, S. Marinel, D. Goeuriot, In situ study on microwave sintering of ZTA ceramic: Effect of ZrO_2 content on densification, hardness, and toughness, J. Am. Ceram. Soc. 100 (2017) 929-936. https://doi.org/10.1111/jace.14658.

[31] J. Samuels, J.R. Brandon, Effect of composition on the enhanced microwave sintering of alumina-based ceramic composites, J. Mater. Sci. 27 (1992) 3259-3265. https://doi.org/10.1007/BF01116022.

Tables' and figures' captions

Table 1: Average particle size and chemical composition of the Al_2O_3 as-received powder (data from the supplier)

Table 2: Average particle size and chemical composition of the 3Y-TZP as-received powder (data from the supplier)

Table 1: Description of the different sintering cells used in this work for the MW thermal cycles

Table 2: Green and sintered relative densities of the Al_2O_3 and 3Y-TZP pellets

Table 3: Temperatures at which a relative density of 75% is reached during sintering with the three sintering cells and difference between these temperatures

Table 4: Emissivity ratio *k* for the 3Y-TZP pellets in the case of the three sintering cells

Figure 1: Schematic of the sintering cell used to sinter the samples in the MW cavity

Figure 2: Evolution of powers and temperature vs time during sintering of the Al_2O_3 samples: (a) effect of susceptor and (b) effect of the mullite tube

Figure 3: Evolution of powers and temperature vs time during sintering of the 3Y-TZP samples: (a) effect of susceptor and (b) effect of the mullite tube

Figure 4: Densification curves with the three sintering cells for the (a) Al_2O_3 and (b) 3Y-TZP samples

Figure 5: SEM micrographs of the sintered Al_2O_3 samples at the surface (black frame) and in the center (red frame) of the sample, sintered with the sintering cells (a, d) SM, (b, e) M and (c, f) S

Figure 6: SEM micrographs of the sintered 3Y-TZP samples at the surface (black frame) and in the center (red frame) of the sample, sintered with the sintering cells (a, d) SM, (b,e) M and (c,f) S

Figure 7: Al_2O_3 and 3Y-TZP average grain sizes in the center and at the surface of the samples for the different sintering cells

Table 3:

Particle size (µm)	Na (ppm)	Si (ppm)	Fe (ppm)	Ca (ppm)	K (ppm)
0.125	10	5	5	4	15

Table 4:

Particle size (μm)	**Y_2O_3 (wt%)**	**HfO_2 (wt%)**	**Al_2O_3 (wt%)**	**SiO_2 (wt%)**	**Fe_2O_3 (wt%)**	**Na_2O (wt%)**
0.04	5.2± 0.5	<5.0	0.1~0.4	≤ 0.02	≤ 0.01	≤ 0.04

Table 5:

Name	Type of sintering cell
SM	Presence of the SiC ring and the mullite tube
M	Presence of the mullite tube and absence of the SiC susceptor
S	Presence of the SiC susceptor and absence of the mullite tube

Table 6:

Samples	**Sintering cells**	**ρ_0 (%)**	**ρ_f (%)**
	SM	52.5	98.3±0.6
Al_2O_3	M	52.0	97.5±0.2
	S	53.1	98.5±0.4
	SM	51.5	98,6±0.6
3Y-TZP	M	52.4	97.6±0.3
	S	52.2	98.7±0.1

Table 7:

Samples	$\mathbf{T_{75\%\text{-}SM}}$	$\mathbf{T_{75\%\text{-}M}}$	$\mathbf{T_{75\%\text{-}S}}$	$\mathbf{\Delta T_{M\text{-}SM}}$ $=T_{75\%\text{-}M}-T_{75\%\text{-}SM}$	$\mathbf{\Delta T_{S\text{-}SM}}$ $=T_{75\%\text{-}S}-T_{75\%\text{-}SM}$
Al_2O_3	1333	1398	1507	66	174
3Y-TZP	1291	1302	1480	11	189

Table 8:

Sintering cells	SM	M	S
Emissivity Ratio *k*	0.955	0.959	1.111

Figure 8:

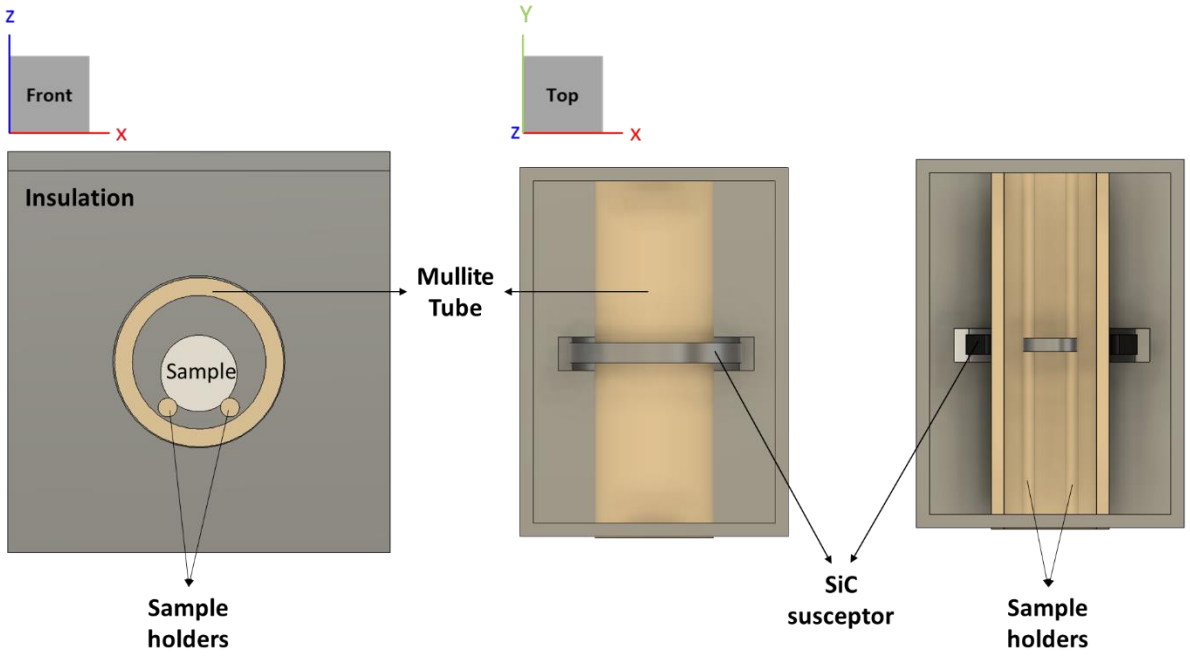
Z
Front
X
Y
Top
Z
X
Insulation
Sample
Mullite
Tube
Sample
holders
SiC
susceptor
Sample
holders

Figure 9:

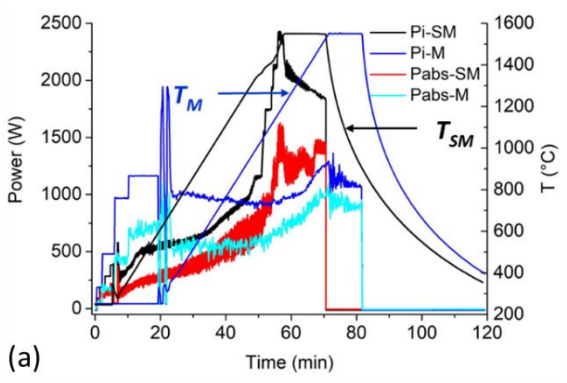
Power (W)
T (°C)
Time (min)
Pi-SM
Pi-M
Pabs-SM
Pabs-M
T_M
T_{SM}
(a)

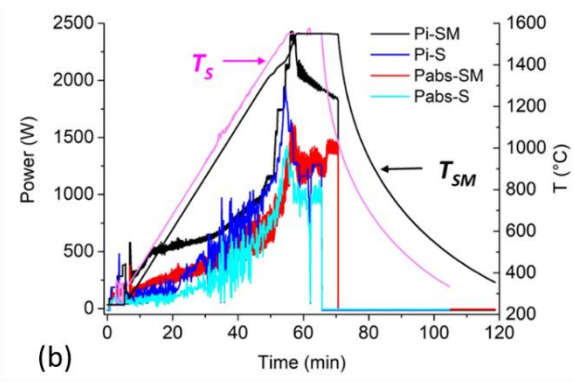
Power (W)
T (°C)
Time (min)
Pi-SM
Pi-S
Pabs-SM
Pabs-S
T_S
T_{SM}
(b)

Figure 3:

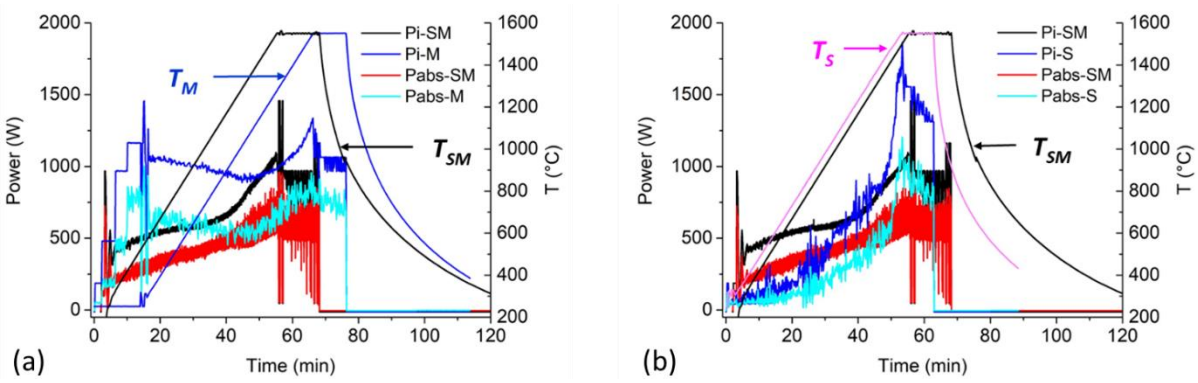
Power (W)
T (°C)
Time (min)
Pi-SM
Pi-M
Pabs-SM
Pabs-M
T_M
T_{SM}
(a)
Pi-SM
Pi-S
Pabs-SM
Pabs-S
T_S
T_{SM}
(b)

Figure 10:

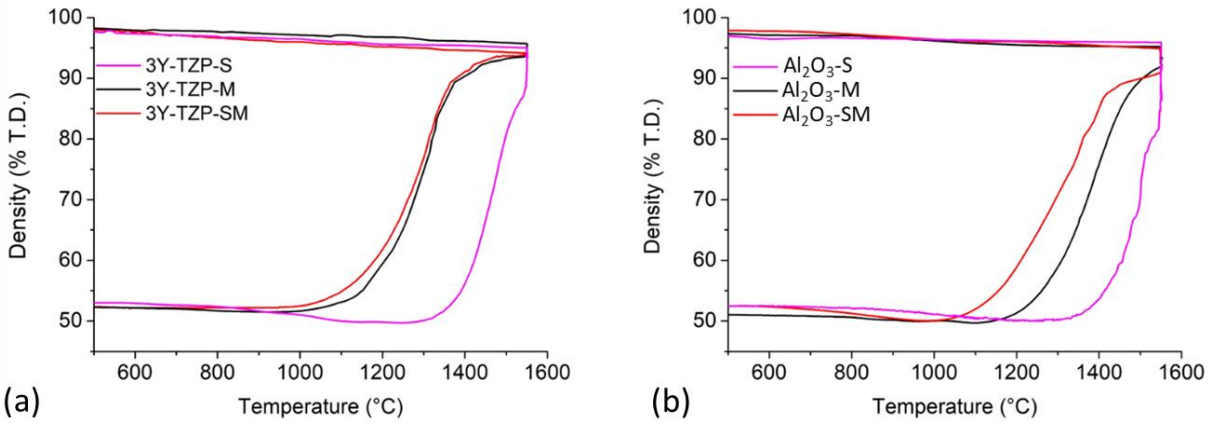
100
90
80
70
60
50
Density (% T.D.)
3Y-TZP-S
3Y-TZP-M
3Y-TZP-SM
600
800
1000
1200
1400
1600
Temperature (°C)
(a)
100
90
80
70
60
50
Density (% T.D.)
Al2O3-S
Al2O3-M
Al2O3-SM
600
800
1000
1200
1400
1600
Temperature (°C)
(b)

Figure 11:

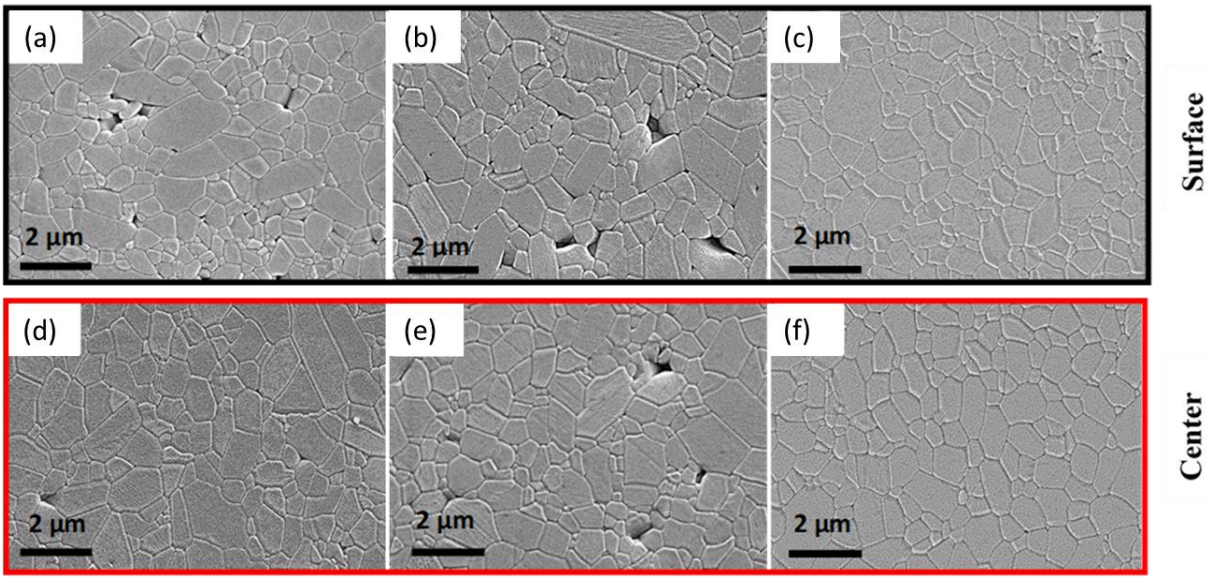

Figure 12:

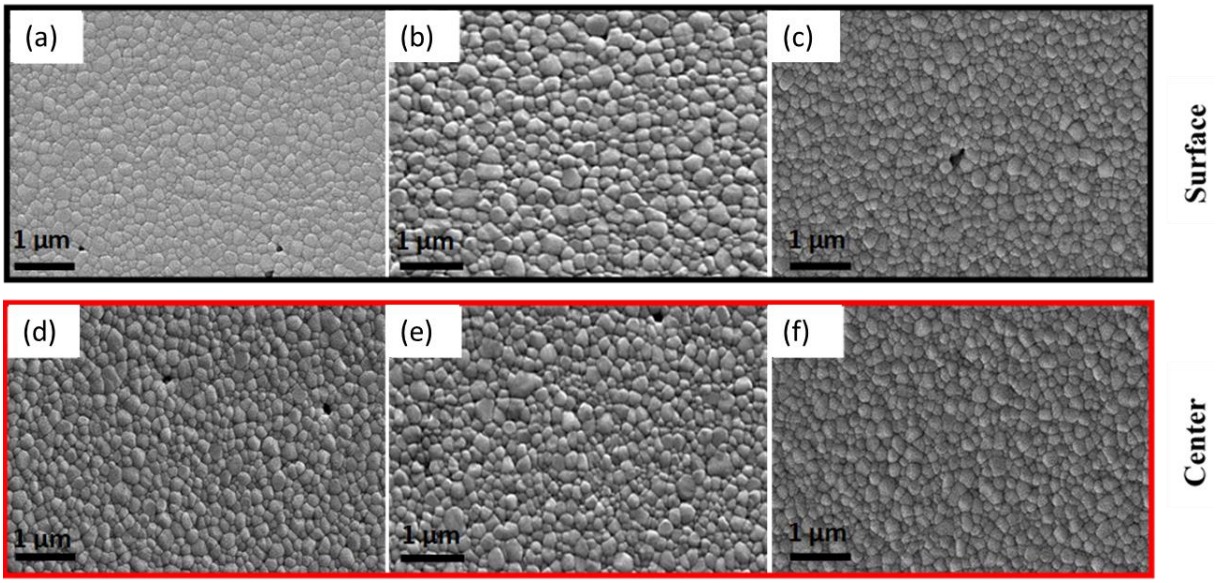

Figure 13:

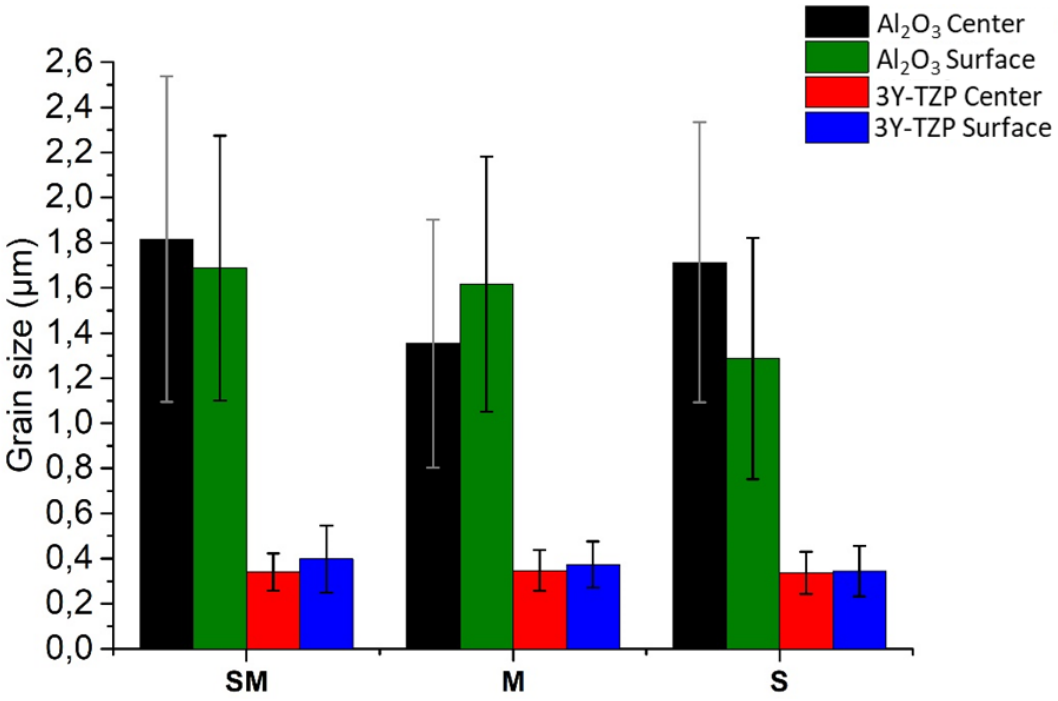
Al2O3 Center
Al2O3 Surface
3Y-TZP Center
3Y-TZP Surface
Grain size (µm)
2,6
2,4
2,2
2,0
1,8
1,6
1,4
1,2
1,0
0,8
0,6
0,4
0,2
0,0
SM
M
S